JOURNAL OF CATALYSIS 156, 120–131 (1995)

Morphological Transformation of Pd Thin Film Catalysts during 1,3-Butadiene Hydrogenation: An Air and UHV STM Study

King Lun Yeung, Kong Hean Lee, and Eduardo E. Wolf[1]

Department of Chemical Engineering, University of Notre Dame, Notre Dame, Indiana 46556

Received September 15, 1994; accepted May 18, 1995

The surface morphology of supported Pd/graphite film catalysts imaged by scanning tunneling microscopy (STM) shows that the microstructure is strongly dependent on the pretreatment and reaction conditions. Results obtained from the ultrahigh vacuum STM have validated the ambient STM images provided the film structures are sufficiently larger than 10 nm. Significant morphological changes occurring during reaction were accompanied by alteration in the activity and selectivity. Three Pd/HOPG films were prepared by exposure to different treatment conditions. It was found that the films with different microstructure exhibit different catalytic behavior, whereas the two films with similar structures prepared by different procedures have similar activity and selectivity. © 1995 Academic Press, Inc.

INTRODUCTION

Understanding the structural effect on catalysts during pretreatment and reaction is important in fundamental catalysis. Many catalytic surfaces experience dynamic transformations under most of the treatment and reaction conditions (1–3), as is evident from the sintering and redispersion processes observed in supported catalysts (4) and surface reconstruction in single crystal surfaces (5, 6). Adsorbate-induced surface structural changes are also observed in thin films that resemble supported catalysts (7, 19). Thus, it is important to know how a reaction induces changes on the surface microstructure and how such changes effect the catalytic activity and selectivity. A knowledge of the relationship between reaction environment and catalyst morphology can be useful in extrapolating information obtained under ideal conditions (i.e., single crystals at ultrahigh vacuum (UHV)) to applications at elevated pressure on supported catalysts. Furthermore, if a strong correlation between structure and activity exists, one may in principle predict the activity–selectivity behavior of the catalyst based on the known surface structure and composition. For this purpose, it is important to know the level of resolution sufficient to validate such a correlation. Atomic resolution is required to identify the active sites and detailed reaction mechanism, whereas microstructural information relates to the distribution of active sites.

Our previous scanning tunneling microscopy (STM) studies have shown that supported Pt and Pd catalysts on graphite (8, 9) have complex morphologies and exhibit both size and shape distributions (8, 11). The crystallite morphology is strongly dependent on the precursor (9–11), support (12), preparation method (10, 11), and treatment history (8). Due to those complicating factors, even such model-supported catalysts (8–12) are difficult to study. Aiming at studying a simpler surface, we turned our attention to thin film catalysts.

We have shown in a recent study (1) on supported Pd thin film catalysts that both treatment temperature and adsorbate gases can have a strong influence on the surface microstructure. Gases that have strong interaction with palladium surfaces, such as hydrogen and hydrocarbons, cause greater structural changes than an inert gas such as helium. Exposure of a Pd film to different C_4 hydrocarbons (*n*-butane, 1-butene, and 1,3-butadiene) shows that surface reaction (*n*-butane dehydrogenation) can result in significant structural changes.

In this paper, we examine the effect of the reaction on the film microstructure using STM, under both ambient and UHV conditions, and measure the resulting changes in catalytic activity. The transformation of surface microstructure of Pd thin film catalysts during 1,3-butadiene hydrogenation reaction and the consequent changes in conversion and selectivity were investigated. Three film microstructures were also prepared to compare their kinetic behavior during the hydrogenation reaction.

EXPERIMENTAL

Thin Film Preparation and Treatment

A thin film, about 20 nm thick, was prepared by evaporating 14 mg of a Pd wire in a vacuum of 1×10^{-6} Torr

[1] To whom correspondence should be addressed.

0021-9517/95 $12.00

(Denton DV-502) onto a highly oriented pyrolytic graphite (HOPG). Six samples (1.2 × 1.2 cm^2) were prepared in each batch of depositions by placing them in a tilted (30°) platform to allow uniform deposition of the metal. Five samples (0.6 × 1.2 cm^2) were used in the study, and STM studies of the fresh films show that they have similar surface structures. Prior to the hydrogenation reaction, the supported thin film catalysts were pretreated in flowing hydrogen at 523 K for 3 h.

Activity and Selectivity Measurements

The reactivity and selectivity of the thin film catalysts (0.72 cm^2/sample) were measured during the hydrogenation of 1,3-butadiene. This reaction was chosen because of its structure sensitivity and high reactivity which permits one to obtain high conversion on a low area model film catalyst. The hydrogenation was conducted in a quartz-tube flow reactor (0.8 cm i.d.) at a constant flowrate of 110 ml/min. The reactant mixture consists of 1,3-butadiene and hydrogen, with nitrogen as diluent gas. The partial pressure of the 1,3-butadiene was kept constant at 4 Torr under an overall reactor pressure of 1 atm. The hydrocarbon reactant and products, 1,3-butadiene, *n*-butane, 1-butene, *cis*-2-butene, and *trans*-2-butene, were separated using a 0.19% picric acid/graphpac chromatographic column (Alltech Associates, Inc.) and their concentrations were monitored using a gas chromatograph (Varian Aerograph 1400) equipped with a flame ionization detector. Blank runs using the graphite support were also performed and there are no detectable products under the reaction conditions presented in this paper.

The study is divided into two parts. First, we investigated the effect of reaction environment on the Pd film microstructure and the consequent changes in catalytic performance. An ambient STM was used for this purpose, while a UHV STM was used to validate some of these results.

Starting with a fresh Pd film, the catalyst was pretreated in hydrogen at 523 K for 3 h, then was exposed to a stepwise increase in reaction temperatures at a fixed H_2/HC ratio of 125. The experimental sequence (Scheme 1) is as follows: the reduced film was allowed to react and equilibrate at a selected temperature for 90 min, and the conversion and product selectivity at that temperature were recorded. Subsequently, the reactor was cooled to 323 K and the catalyst activity and selectivity at that temperature were also measured. Thereafter, the reactor was quenched to room temperature and flushed with flowing N_2 prior to removal of the catalyst for STM analysis at ambient conditions. After STM imaging, the film catalyst was loaded back into the reactor for further studies at other reaction temperatures. Since the catalyst was exposed to air during STM imaging under ambient conditions, it was flushed with N_2 and then H_2 at room temperature prior to the next reaction step to minimize the effect of ambient gases. Higher temperatures were not used during flushing because they could result in microstructural transformations (1). The procedure was then repeated for the next reaction temperature.

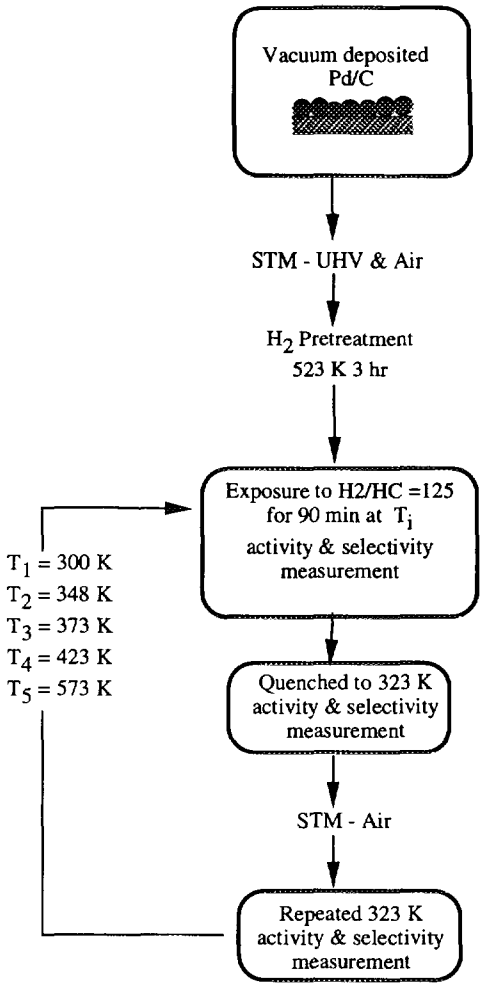

SCHEME 1. Experimental schematic. The fresh evaporated Pd/C film was treated in H_2 followed by exposure to reactions with stepwise temperature increase. The film was then cooled down to 323 K for activity and selectivity measurement followed by STM imaging.

In addition to the experiments conducted in the flow reactor, the hydrogenation reaction at 300 K was also performed in a reaction chamber (2.75 in. 6-way cross) attached to the UHV STM chamber as shown in Fig. 1. This enabled us to image postreaction samples without exposure to ambient gases. The pretreated catalyst (H_2 at 523 K for 3 h) was transferred to the reaction chamber through a loadlock fast-access door and the reaction mixture was introduced via a leak valve until the same gas composition as in the flow reactor was attained. After reaction, the chamber was evacuated using a turbomolecular pump to 3 × 10^{-7} Torr and the sample was transferred

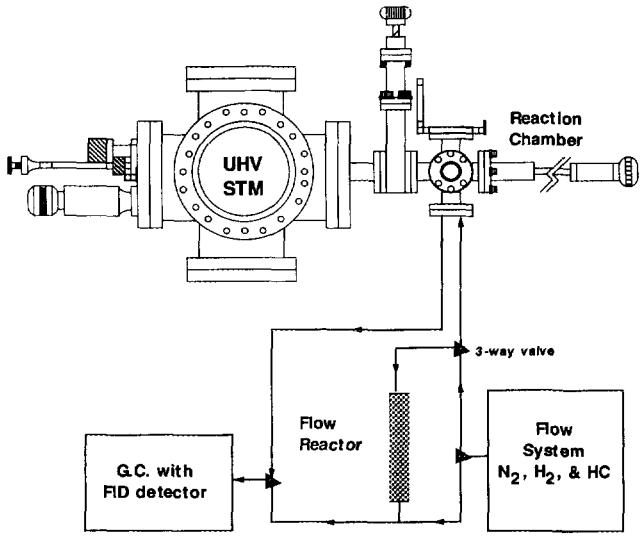

FIG. 1. UHV STM schematic diagram. The UHV STM is housed in an 8-in. 6-way cross which is attached to the reaction chamber (2.75-in (6-way cross) with heating capability. Various reactive gases can be lead to the chamber and then delivered to a GC with FID detector for analysis.

to the STM sample stage in the UHV chamber using a linear motion feedthrough.

For the second part of the study, three film microstructures were prepared using different methods and their conversion and selectivity toward 1,3-butadiene hydrogenation were determined at different reaction temperatures. The first film structure (R125) was obtained using a similar procedure, as shown in Scheme 1, i.e., reaction at H_2/HC ratio of 125 up to 473 K, for 90 min, but without exposure to ambient gases, which resulted in one of the stable microstructures. The second film microstructure (R10) was formed upon further exposure of a R125 film to a low H_2/HC ratio of 10 at 473 K. A third film (HAn) was prepared by high-temperature (723 K) annealing of a fresh Pd film in hydrogen for 60 h. The R125 film structure was stable for temperatures less than 473 K and H_2/HC ratios greater than 25, whereas the other two films (R10 and HAn) were stable between 300–473 K for H_2/HC ratios $\geq$4.0.

STM Imaging

The two STM used in this study were an ambient STM (Nanoscope II, Digital Instruments) and UHV STM (Burleigh, Inc). The ambient and UHV STM have effective scan ranges of 7500 and 5400 nm, respectively, and were operated in the height imaging mode to provide good topological images. To avoid undesirable tip effects (e.g., multiple and unstable tips), only Pt/Ir STM tips that can achieve atomic resolution on HOPG were used. After each run, the tips were re-evaluated in a similar manner to determine possible tip deterioration during STM operation. The operational bias voltage was kept between 15 and 150 mV with the tunneling current fixed at 1 nA. The horizontal scan frequency was maintained below 5.0 Hz for best image resolution.

At least four different areas on a sample were selected for STM analysis, generally in the center and halfway between each corner of the sample and the center. Usually, all the scanned areas yielded similar structures. While the micrographs presented are the best resolved, they are definitely representative of all other four to five scanned areas. Each area was carefully mapped by moving a fixed scan window (1000^2 or 500^2 nm^2) in a raster pattern. Depending on the scale of surface features to be examined, smaller or larger scan windows were also used. Prominent surface features such as grains and facets are described by their geometrical shape and size. Surface roughness, standard deviation in height, and fractal dimension are also calculated to obtain a quantitative description of the surface.

X-Ray Photoelectron Spectroscopy

X-ray photoelectron spectroscopy (XPS) was used to characterize the surface composition of the Pd film samples. The studies were performed using a spectrometer from Kratos Analytical, Inc., with a monochromatic Mg$K\alpha$ radiation source ($h\nu$ = 1253.6 eV). The base pressure of the instrument was $<1 \times 10^{-9}$ Torr. The electron binding energy was calibrated by assigning C 1s to be 284.6 eV. Samples were analyzed as received after treatment in the reactor to determine if exposure to ambient gases could be detected by XPS. No special pretreatment was used in the XPS chamber to avoid introducing additional surface changes. Of particular interest was to detect the formation of Pd oxide.

Materials

The Pd wire used in the film preparation is 99.999% pure (Johnson–Matthey, AESAR), and the HOP graphite is ZYH grade (UCAR Carbon Company, Inc.). The hydrogen and nitrogen gases used in this study are of UHP quality (Linde Union Carbide) while the 1,3-butadiene is 99.5% pure and is supplied by Matheson Gas Products.

RESULTS

I. Ambient STM versus UHV STM

Due to the roughness of the film surfaces, especially after reaction, it was difficult to obtain a statistically significant set of data at atomic resolution to categorize each surface structure. Thus, we decided to correlate the transformations of the observed microstructure to the changes in catalytic activity to give at least a qualitative correlation between microstructure and catalyst performance.

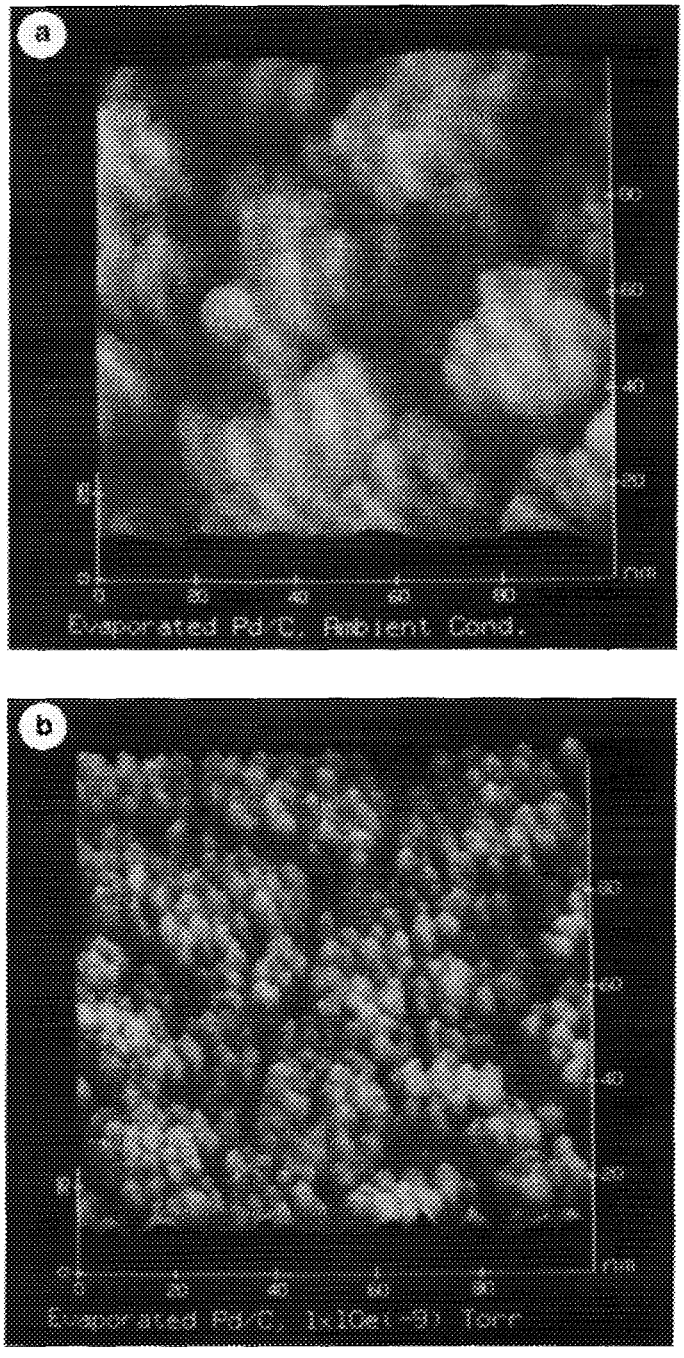

FIG. 2. STM images of the surface structure of fresh Pd film (a) in air and (b) in UHV.

Figure 2 compares the microstructure of an unreacted Pd thin film on graphite imaged with STM under ambient (Fig. 2a) and UHV (Fig. 2b) conditions. The ambient STM image shows a 20-nm thick film made up of multiple layers of uniformly packed Pd grains (10 nm). Similar film microstructure was imaged by the UHV STM at 10^{-9} Torr as shown in Fig. 2b. To preserve the film structure, no special cleaning method (i.e., heating or sputtering) was used on these fresh samples. Nonetheless the evacuated film should be cleaner than at ambient conditions and at least free from physisorbed species. In addition, the image (Fig. 2b) also reveals the columnar Pd growth common for the films deposited from vapor deposition at an oblique angle and under low substrate temperature. Images on the other five samples prepared from the same batch of the Pd film showed a similar and reproducible microstructure. Humbert *et al.* (14) reported that only when Pd particles are less than 10 nm does exposure to ambient gases have a significant effect on the particle morphology. This was also confirmed by the reproducibility of the images of samples left at ambient conditions for extended periods of time.

After hydrogen pretreatment (523 K, 3 h) an order-of-magnitude increase in grain size (10 to 110 nm) was observed, in good agreement with our previous work (1). Subsequently, exposure of the Pd film to reactant gases at room temperature (300 K) gives the film microstructure shown in Fig. 3a. Film fragmentation is common and the film exhibits broader size distribution and grains with irregular shapes resulting in an increase in surface roughness. A similar experiment was conducted in the reaction chamber attached to the UHV STM system (Fig. 1) without exposure of the film to ambient gases during STM imaging. Again, the film microstructure (Fig. 3b) is similar to that imaged by ambient STM (Fig. 3a). This indicates that, at the microstructural level resolution of these micrographs, ambient gases have only a small effect on the microstructure of the film. All the subsquent micrographs presented in this paper were obtained in ambient STM.

XPS measurements (Table 1) conducted on reacted Pd films indicate that after exposure to ambient gases the Pd 3*d* binding energy (BE) was within 0.1 eV of the value for metallic Pd (334.9 eV). Weakly bound oxygen, presumably from surface moisture, and graphitic carbon from the reaction were also detected. Although these adsorbates can alter the local atomic structure, their presence does not seem to have an apparent effect on the microstructure in comparison to exposure to the reactants at reaction temperature.

II. Microstructural and Activity Transformation under Reaction Environment

Figure 4 shows the microstructural transformations of a Pd thin palladium film occurring when it is used as a catalyst for the 1,3-butadiene hydrogenation reaction following the experimental procedure outlined in Scheme 1. Exposure to reaction at $T = 348$ K results in the formation of facet-like structures shown in Fig. 4a. Large areas of the palladium film exhibit rectangular facets (aspect ratio = 1.8; see arrows in figure), which have an average size of 350×200 nm^2 and are made up of sintered grains decor-

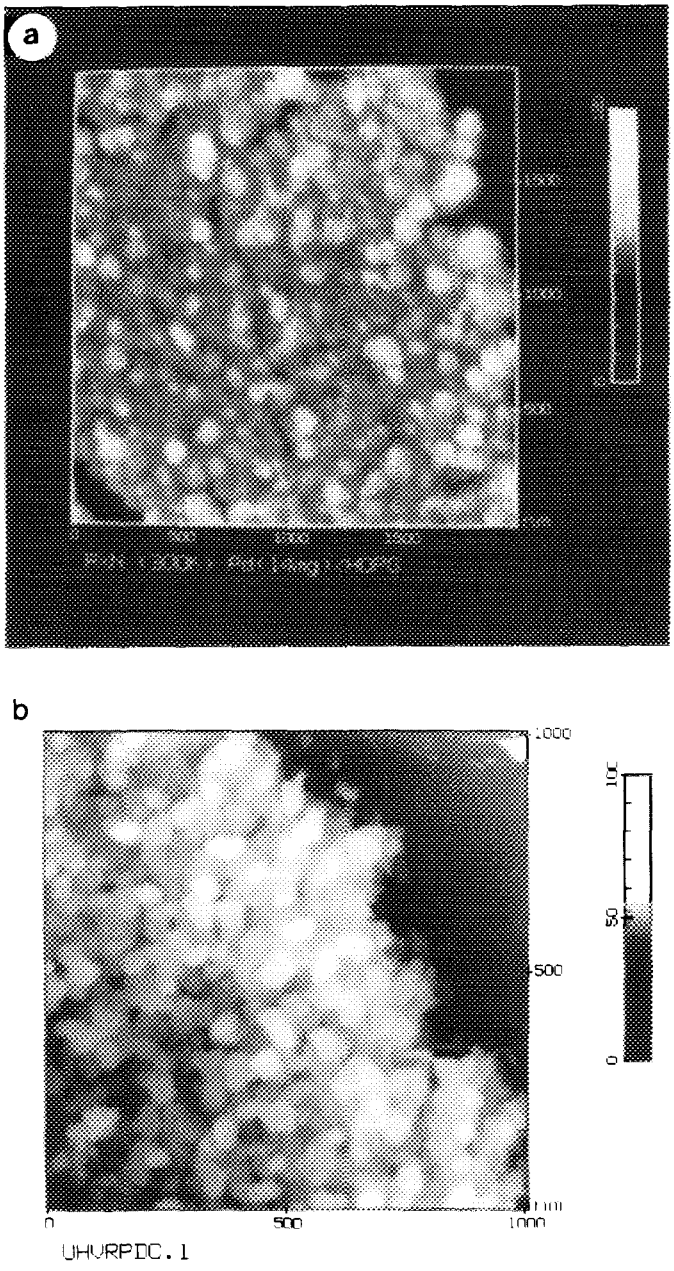

FIG. 3. Pd/C film structure after exposure to the reactive hydrogen/1,3-butadiene mixture at 300 K imaged (a) in air and (b) in UHV.

ated by smaller particles. This transformation from the microstructure shown in Fig. 3 was stable for temperatures less than 348 K. After exposure to reaction at 373 K, the smooth trapezoidal facets (180 × 200 nm^2; see arrows in figure) shown in Fig. 4b replace the rectangular facets of Fig. 4a. Further reaction at 423 K results in disappearance of facets and occurrence of local sintering resulting in the porous film structure shown in Fig. 4c. The measured grain size is 175 nm, smaller than the facets. Formation of 250 nm aggregate clusters (Fig. 4d) occurs after exposure of the film to reaction at 473 K. The maximum reaction temperature used was 473 K to prevent carbon deposition as indicated by the rapid catalyst deactivation and the loss of resolution in the STM.

The conversion and product selectivity of the different film microstructures shown in Fig. 4 were measured at the same temperature of 323 K to determine the relationship between microstructure and catalyst activity. Figure 5a shows the butadiene conversion at 323 K for the different exposure temperatures leading to various film microstructures shown in Fig. 4. Results obtained pre- (open squares) and post- (solid dots) STM imaging are also shown to demonstrate the reproducibility of the measurements. The results indicate an initially low conversion that increases by twofold after changes in the film microstructures shown in Figs. 4c and 4d. The results also show that, like the film microstructure, conversion is not affected by exposure to ambient gases during STM imaging. Figure 5b displays the product selectivity results corresponding to Fig. 5a. Selectivity to *cis*-2-butene is structurally insensitive and remains unaffected during the film transformation. For 1-butene and *trans*-2-butene, there is data scattering at low temperatures. However, the general trend indicates that facets (Figs. 4a and 4b) consistently favor the production of *trans*-2-butene, while the more open film microstructures (Figs. 4c and 4d) preferentially produce more 1-butene (~20%).

Besides describing the prominent surface features in terms of their geometry and size, we attempted to quantify the surface microstructure using the surface roughness and fractal dimension estimated from the STM images. Surface roughness (f) was calculated from the ratio of the actual surface area to the projected area (i.e., f = surf. area/scan area). Average height and standard deviation were also used to measure surface roughness. The average height (h) was obtained over the 160,000 data points from each images, and the standard deviation (σ) was calculated assuming a gaussian distribution. The fractal dimension (D_f) of the surfaces was obtained from the slope of the log–log plot of the surface area versus scan size. For an ideal flat two-dimensional surface, f is independent of scan size and the slope of the log–log plot should equal to 2.0.

Table 2 summarizes the grain size, height, σ, f, and D_f for various exposure temperatures. The surface roughness

TABLE 1

Binding Energy of the Surface Elements of the Reacted Pd/C Films

Element:	Pd 3*d*	C 1*s*	O 1*s*
Binding energy:	335.0 eV	284.6 eV	531.7 eV

Note. Reference: C 1*s* = 284.6 e V.

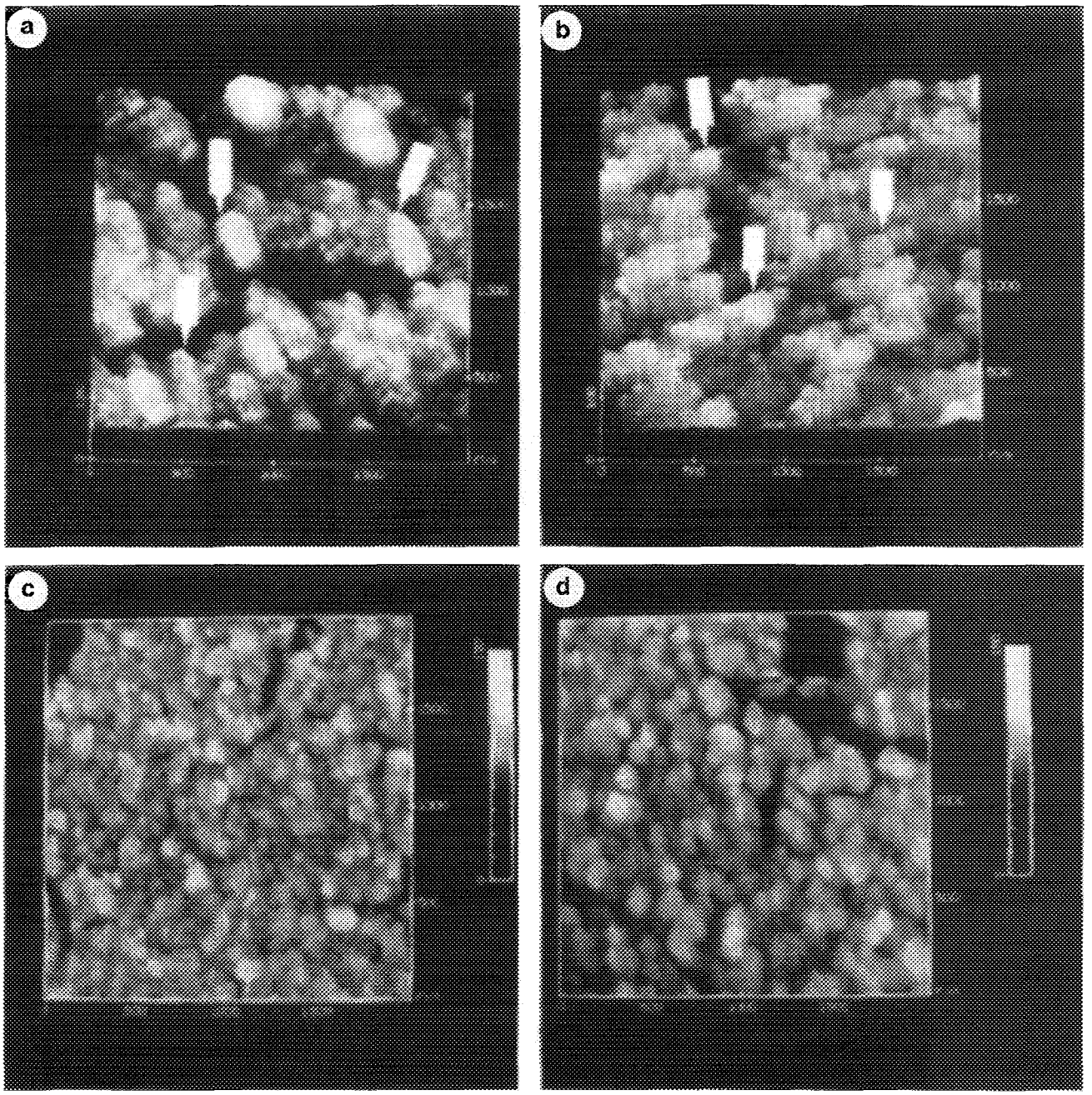

FIG. 4. Pd/C film structure after exposure to the reactive hydrogen/1,3-butadiene mixture (H_2/HC = 125) at increasing temperatures; (a) 348 K, (b) 373 K, (c) 423 K, and (d) 473 K. Arrows have been added in some images to aid the description of the micrograph.

(f) was obtained at a fixed scan size of 100 nm since f changes with scan size as indicated by the fractal dimension, D_f. The fresh Pd film is made up of small grains (10 nm), and the measured surface roughness (f) is 1.18. As the facetlike structures and trapezoids are formed, f decreases from 1.18 to 1.02 and 1.09 reflecting the smoother film surface. Similarly, growth in grain size also diminishes the surface roughness, f. It is important to note that f, σ, and D_f were measured from the STM images and account only for the topmost surface layer of the film that is probed by the STM. Although these techniques are useful in assigning numerical values to each microstructure, they contain limited information to fully represent the actual surface. Until better techniques are developed, we can only state qualita-

TABLE 2

A Summary of the Grain Size, Grain Height, σ f, D_f and TON of the Pd/C Films after Various Exposing Temperatures

Samples	Thickness (nm)	Features	Size (nm)	Height (nm)	SD (nm)	f (100 nm)	D_f	TON
Pd(14)	20	grains	10	20.36	4.07	1.18	1.8932	
300 K		grains	110	27.28	4.98	1.08	1.9885	3.7
348 K		facet-like	350 × 200	21.22	4.01	1.02	1.9945	4.24
373 K		trapezoids	180 × 200	25.51	4.71	1.09	1.9732	2.67
423 K		grains	175	46.97	6.68	1.06	1.9839	8.54
473 K		cluster aggregates	250	51.36	5.46	1.06	1.9529	9.95

Note. Deposition rate 1.3×10^{19} Pd/s.

tively how the reaction environment affects the surface microstructure and its consequent effect on both activity and selectivity.

Nonetheless, a turnover number, TON (no. C_4H_6 molecules/Pd atoms-s), was estimated based on the surface area estimated by multiplying the surface roughness times the geometrical area of the film, assuming a surface atomic density of 1.05×10^{15} Pd/cm^2, corresponding to a polycrystalline foil (15). The TON increased with increasing grain size, confirming the results shown in Fig. 4a.

III. Microstructure and Catalyst Activity and Selectivity

The previous section has shown the microstructural transformation occurring on a Pd thin film during the 1,3-butadiene hydrogenation reaction. Changes in conversion and product selectivity were observed to coincide with the transition from one microstructure to the other. In this section, the kinetics of 1,3-butadiene hydrogenation on three palladium film microstructures is presented. A film (R125) with a microstructure similar to that shown in Fig. 4d was prepared using the same procedure (see Scheme 1) but without exposure to ambient gases, since no intermediate STM images were obtained in this case. Figure 6a shows the same aggregate clusters of size and shape comparable to those shown in Fig. 4d, indicating that the procedure gives reproducible microstructure. In addition, the activity of the R125 film is similar to that of Fig. 5a, giving a 4.0% conversion at 323 K. As shown in Fig. 6a, the R125 film exhibits rifts exposing portions of the graphite support. The film thickness measured by STM from the exposed support is about 50 nm, about twice as thick as the original film.

A second film structure, referred to as R10, was prepared by exposure of a R125 film to reaction at 473 K but at a lower H_2/HC of 10. After the reaction, the aggregate clusters of R125 (Fig. 6a) were transformed into the dendritic microstructure shown in Fig. 6b. The dendritic film exhibits branches of 180 nm length and 50 nm width and their measured thickness is about 30 nm. The film has a calculated fractal dimension of 1.7. This microstructural transformation was also accompanied by a decrease in conversion from 4.0 to 2.4% (T = 323 K, H_2/HC = 125).

Another dendritic film microstructure (HAn) was prepared using a completely different pathway by annealing a fresh Pd film in hydrogen at 723 K for 60 h. Figure 6c shows that this film also exhibits dendritic characteristics in the form of narrow palladium bridges interconnecting several palladium islands. The annealed film closely resembles the R10 film and has the same fractal dimension of 1.7. These three film microstructures were stable under the reaction conditions ($T \leq$ 473 K, H_2/HC = 125) used in this study and exhibit reproducible reaction data.

Conversion versus temperature and Arrhenius plots for the three films are shown in Fig. 7. Figure 7a shows that at any given temperature, the butadiene conversion of R125 film is higher than that of either R10 or HAn, both of which have essentially the same conversion. Arrhenius plots of reaction rates are linear, as shown in Fig. 7b. The calculated activation energies are 14.0, 4.8, and 5.1 kcal/gmol for R125, R10, and HAn, respectively. The decrease in the activation energy from R125 to R10 films is indicative of a change in the reaction pathway resulting from the microstructural transformation of R125 after its exposure to reaction. This is also supported by the significantly different product selectivities of the two film microstructures.

In the previous section, the reaction data (Figs. 3a and 3b) were measured for a single temperature (323 K) to compare the catalytic behavior of the different palladium microstructures resulting from its exposure to the reaction environment. Figure 8a presents the conversion and selectivity data of a palladium film recorded at various reaction temperatures. The data indicate 100% selectivity toward butene products with a small amount of *n*-butane produced at temperatures above 423 K. 1-butene has a maximum selectivity of 80%, whereas *cis*-2-butene exhibits a decrease in selectivity with increasing temperature, reaching a low value of 5% compared to an initial 40%. *Trans*-2-butene is only formed above 348 K and reaches a stable selectivity of about 55%. Clearly, the activity and selectivity are changing as the microstructure changes with increasing exposure temperatures until it reaches a stable level at a temperature of 423 K. Thereafter, the activity and selectivity are reproducible.

The activity and selectivity vs temperature profile for the R125 film is shown in Fig. 8b. The results shown in Fig. 8a are different from those shown in Fig. 8b because the former reflects the microstructural transformations of the film as it reaches the stable R125 structure. Data shown in Fig. 8b are reproducible when compared with a sample similarly prepared. The selectivity in Fig. 8b shows that butenes are the primary product and *n*-butene is formed

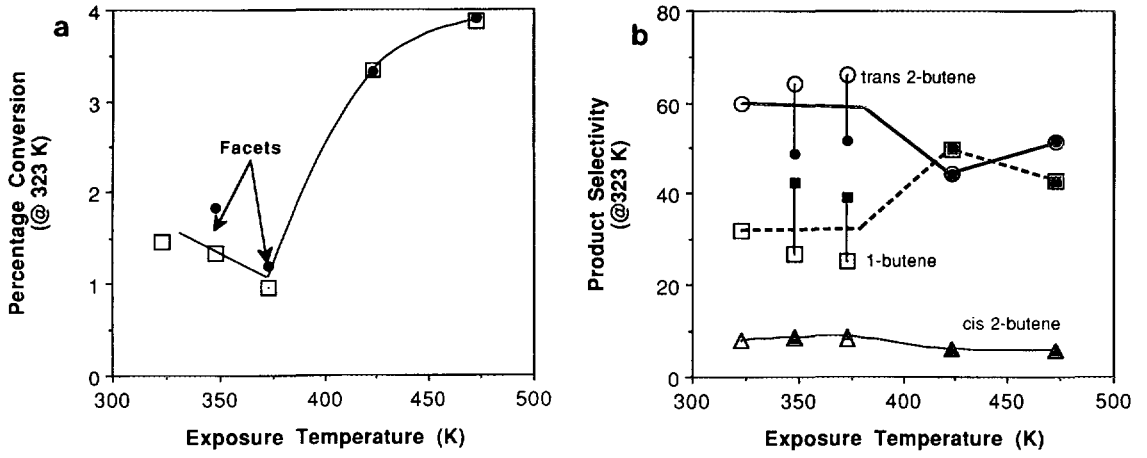

FIG. 5. Activity and selectivity measured at 323 K and H_2/HC ratio = 125 for the different structures: (a) percent butadiene conversion vs treatment time and (b) product selectivity vs treatment time. Open and solid symbols represent activity measurements before and after STM imaging, respectively.

only above 398 K (as is evident by the difference between 100% and total butenes). Initial 1-butene selectivity is 40% and decreases to 10% at higher temperatures. The decrease in 1-butene is observed to coincide with increases in *n*-butane and *cis*-2-butene production. *Trans*-2-butene has a steady-state value of about 50%. The changes in activity and selectivity in R125 are the consequence of the reaction kinetics and are not due to changes in microstructure.

R10 and HAn films, which have similar dendritic microstructures, exhibit essentially the same kinetic parameters, activity, and selectivity profile, but differ from R125 results, as shown in Fig. 8c. These films produce only butene products with steady-state selectivity of about 25% for 1-butene, 65% for *trans*-2-butene, and 10% for *cis*-2-butene.

The results demonstrate that microstructural transformations can occur during reaction (e.g., R125 to R10) and alter the catalytic behavior of the surface resulting in significantly different activation energies and product selectivities. Furthermore, this study has shown that palladium catalysts with different microstructures (R125 vs R10) exhibit different kinetics parameters, whereas similar microstructures (R10 and HAn) exhibit similar kinetics regardless of the treatment history of each catalyst.

DISCUSSION

This work demonstrates several important relations between catalytic activity and selectivity and surface microstructure. We have shown that on Pd thin film ambient and UHV STMs yield similar microstructural results, and exposure of the samples to ambient gases at room temperature do not significantly affect their microstructure or reactivity. We have also clearly demonstrated that catalytic surfaces can be affected by the reaction environment causing microstructural transformations that can alter the activity of the catalyst, resulting in changes in reaction kinetics. In addition, the activity and selectivity of the palladium catalyst to 1,3-butadiene hydrogenation can be *qualitatively* correlated to the film microstructure; different microstructures in general exhibit different catalytic behavior, whereas similar microstructures give similar activity and selectivity.

I. Ambient STM versus UHV STM

Similar microstructures (Figs. 2 and 3) of fresh and reacted Pd/C films were observed with STM under UHV and ambient conditions. Exposure to air during ambient STM imaging leads to adsorption of ambient gases on the film surface. Although UHV conditions do not guarantee an adsorbate-free surface, the UHV STM image shows more detail of the fresh Pd columnar film structure. The grain-size discrepancy for palladium imaged in ambient and UHV can be attributed to adsorbed gases (28), which do not significantly affect the overall film microstructure. This effect of adsorbed gases on the microstructure diminishes rapidly with increasing grain size and was not apparent in the reacted film as shown in Fig. 3. The results indicate that on the Pd/C films, exposure to ambient gases has minimal effect on the film microstructure, especially if the grain sizes are large.

We have also shown that the activity of the reacted films is similar, even if the films were exposed to air prior to the activity measurement. Most adsorbed gases can be removed from the film surface during the low-temperature N_2 flushing prior to reaction, but some chemisorbed ones will probably remain on the surface. These chemisorbed gases are apparently eliminated during the reaction and thus do not affect the resulting microstructure. Reactants

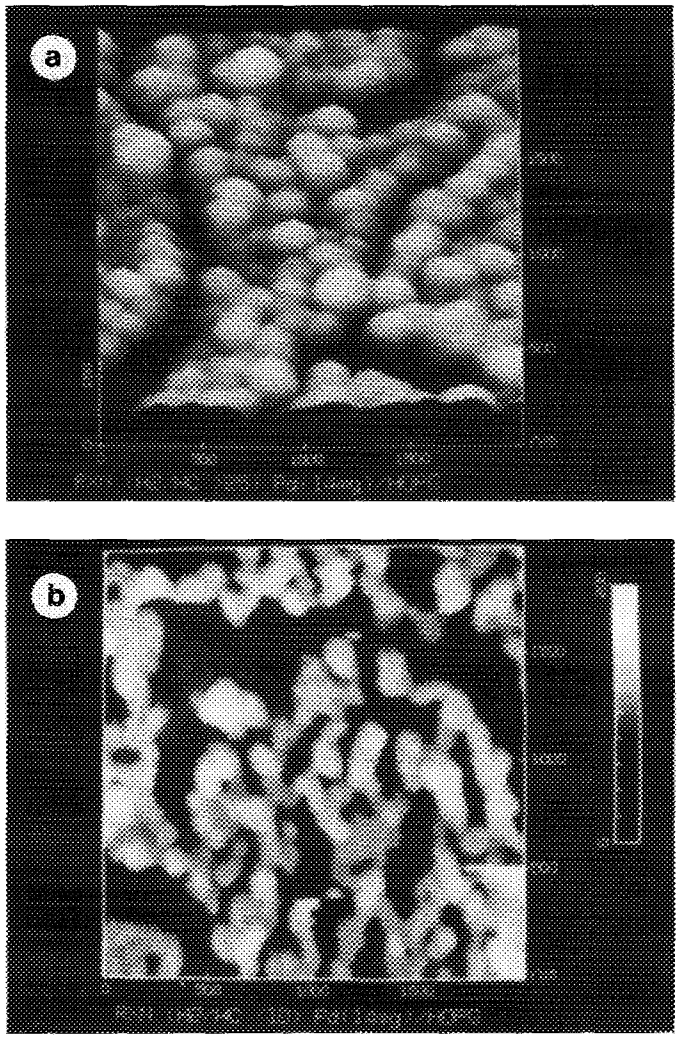

FIG. 6. STM images of (a) R125 film structure after catalyst activation, (b) R10 film structure after exposure of the film to low H_2/HC ratio = 10 at 473 K, and (c) HAn film after hydrogen annealing at 723 K for 60 h.

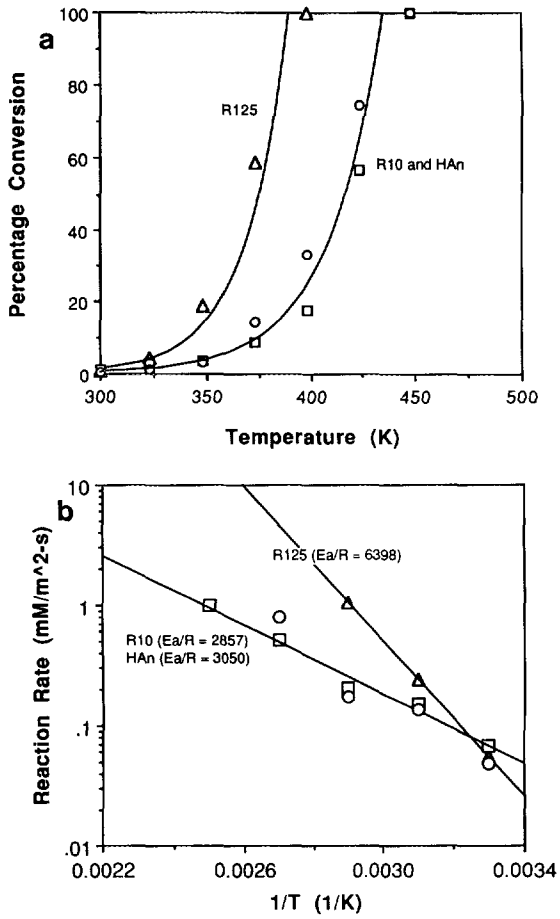

FIG. 7. (a) Percent butadiene conversion vs reaction temperatures for R125, R10, and HAn film structures; (b) Arrhenius plot of reaction rate vs $1/T$(K) for the thre film structures.

such as H_2 and 1,3-butadiene result in a much greater effect on the microstructure than the ambient chemisorbed species. The high H_2/HC ratio during reaction also assists in reducing the Pd surface to its metallic state, if it is ever contaminated during ambient exposure. The XPS results also confirm that PdO is not a significant factor in the observed microstructural transformations and activity results obtained.

II. Microstructural and Activity Transformation under Reaction Environment

We have shown that significant morphological transformations occurring during reaction were accompanied with alteration in the catalysts' activity and selectivity. The method of palladium deposition, i.e., thermal evaporation, onto the cold substrate results in Pd columnar growth (Fig. 2), which is not in thermodynamic equilibrium with the reaction environment. The results show that it was not sufficient to stabilize the film microstructure even after the

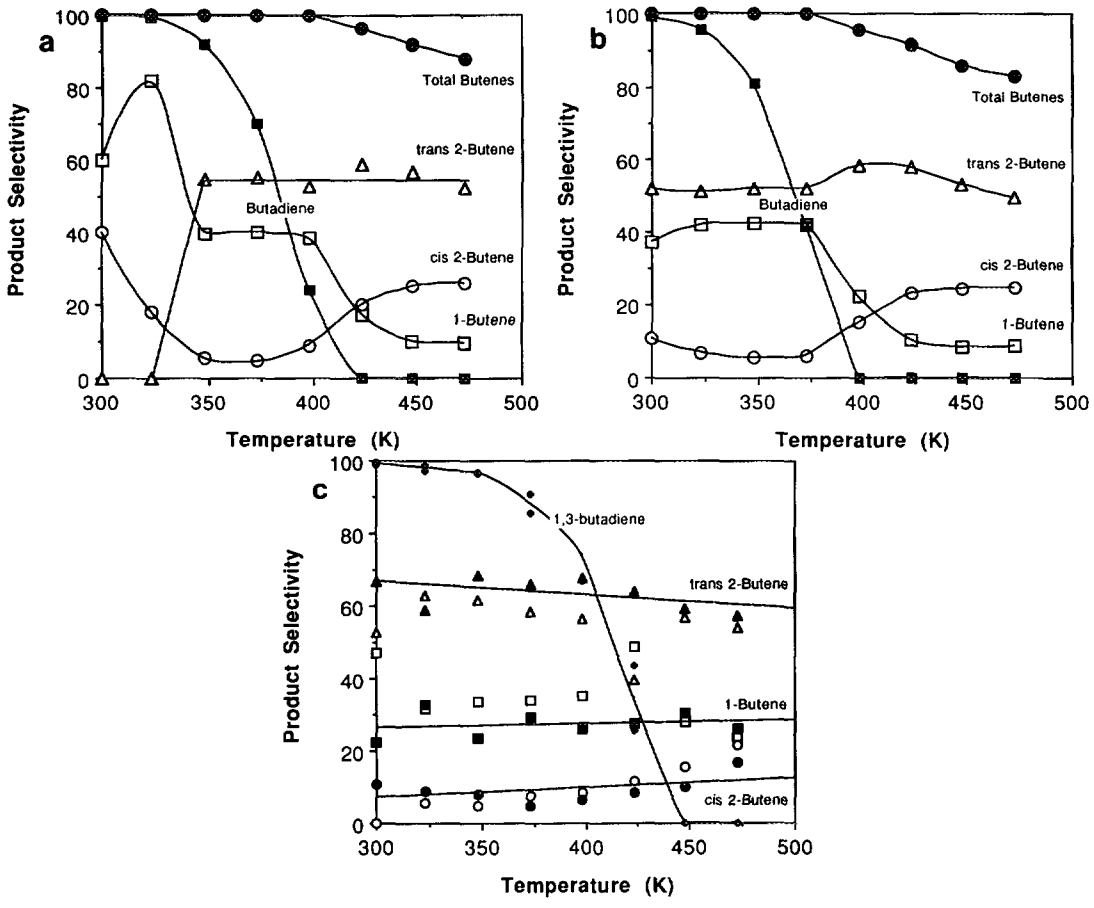

FIG. 8. Product selectivity vs reaction temperatures for (a) film activation, (b) R125 film, and (c) R10 (open diamond) and HAn (solid diamond).

standard pretreatment at 523 K in H_2 for 3 h and that significant changes occur during reaction.

The transformations observed during reaction were more drastic (i.e., occurred faster and at lower temperatures) than those previously observed in the presence of hydrogen alone or C_4 hydrocarbons in the absence of hydrogen (1). During reaction, in addition to the adsorbed reactants, there are adsorbed intermediates, adsorbed products (saturated and C_4 olefins), and by-products (carbon) and hydrocarbon fragments on the surface. These species can alter both local and global surface free energies, causing a more significant effect than single adsorbates.

One can speculate that the presence of adsorbates affects the surface free energy which is minimized by decreasing the exposed surfaces area via sintering. This leads progressively to a more porous film structure that becomes stable for a set of reaction conditions such as the R125 film. One may also question that perhaps the observed transformations are due to the temperature rise during reaction. According to our calculations based on the heat of reaction, local surface heating due to this exothermic reaction is minimal and at most there is a 20°C increase at 90% conversion. Furthermore, during heating in He, an inert environment, morphological transformations did not occur in the temperature range used in this work. Consequently, the temperature rise during reaction should have a negligible effect on the transformations observed.

Other authors (20–22) have also reported remarkable changes in some surface processes such as surface roughening, sintering, and redispersion, when the surface is exposed to reactive gases. Schmidt and co-workers (3) have shown that Pt single crystal spheres used in NH_3, C_3H_8, and CO oxidation reaction and in NH_3 decomposition undergo morphological changes with the formation of facet structures, and the resulting surface morphology is a strong function of the reaction and reactant composition. A recent STM study (13) of the roughening and facet formation on a low area Pt–Rh gauze catalyst also reported strong structural dependence on pretreatment conditions.

The most significant result of this study is the observed activity and selectivity changes that accompanied each microstructural transformation. The measured increase in conversion (Fig. 5a), even though the surface area is actually decreasing (Table 2), strongly suggests that this is

solely a structural rather than a surface-area effect. This is also supported by the significant change in product selectivities (Fig. 5b) during the transformation. These results indicate a strong correlation, albeit qualitatively, between microstructure and catalyst behavior. Clearly, the surface features formed during reaction create new sites which contribute to the change in activity and selectivity.

III. Microstructure and Catalyst Performance

We showed that there is a relationship between structure and activity via changes in the active-site distribution. It is important to note that catalyst surfaces obtained via different treatments in studies involving supported catalyst often yield different activities. What is unique about our results is that the resulting microstructure after a given pretreatment can be determined.

The decrease in conversion from 4.0 to 2.7% at T = 323 K coincided with the transition from R125 (aggregate clusters) to R10 (dendritic) film microstructure. While the microstructural transformation is believed to be solely responsible for the decrease in activity, it is necessary to consider the possible role of catalyst deactivation from carbon deposition (23–25). XPS analysis shows that carbon is always present, even on the films that show an increase in activity after exposure to reaction. Furthermore, the hydrogen annealed film (HAn), which was not exposed to reaction and thus to carbon formation, exhibited a microstructure and activity similar to those of R10. Clearly, carbon formation is not the main factor for the decrease in conversion of the R10 catalyst within the temperature range studied. Instead, the difference in activity between R125 and R10 film is a direct function of microstructure which determines the activity profile of the surface in terms of the numbers and types of active sites available for the reaction.

The above argument is supported by the kinetic results. The activation energy of the R125 film (E_a = 12.7 kcal/gmol) is close to the value reported by Bertolini and coworkers (26, 27) for Pd(111) and Pd(110) of 12.5 and 12.0 kcal/gmol, respectively. However, the dendritic films, R10 and HAn, have similar lower activation energies of 4.8 and 5.1 kcal/gmol, respectively, and lower pre-exponential factors. Besides the significantly different activation energies between the two microstructures (R125 versus R10), they also yield different product distributions. This indicates that the site distributions of the two microstructures are different. The R10 and HAn films obtained from different preparation pathways yield similar microstructures and activation energy. In addition, these films exhibit nearly identical product selectivities. Furthermore, fractal dimension measurement also provides a quantitative agreement of HAn and R10 films with respect to R125 film. This indicates that films of similar microstructure and similar reactivity must have similar distribution of active sites.

The complexity of the surfaces studied has prevented the achievement of atomic resolution and the identification of crystallographical changes. X-ray diffraction is not suitable for the study of thin films and other surface structural characterization was not possible due to the complexity of the surface morphology of the films studied. Currently, we are studying different techniques to quantify surface morphology and are evaluating different characterization tools such as grazing angle XRD, electron diffraction, and other microscopy techniques to complement the STM data and attempt a quantitative correlation. Nonetheless, the qualitative correlation obtained between reactivity and microstructure suggests that it may be possible to categorize a complex surface into finite numbers of known microstructures, each well characterized in terms of both surface and solid structures, and correlate their catalytic behavior toward a specific family of reactions.

The results presented indicate that extreme caution must be exercised when comparing results under different reaction conditions. The results obtained in this work suggest that in general catalytic results can only be extrapolated when the surface microstructures are evaluated and found to be similar and thus have a similar distribution of active sites.

CONCLUSIONS

This paper shows several important results regarding microstructure and catalytic activity: (1) the comparison of STM images under atmospheric and UHV conditions, (2) the effect of reaction environment on a catalytic surface and its reactivity, and (3) the demonstration of a relationship between structure and activity via changes in the active-site distribution.

Most of the STM atomic resolution images to date have confirmed results obtained by other techniques such as LEED under UHV conditions and have also contributed many new and important discoveries that have increased our understanding of surfaces. Our STM results indicate that the surface microtructure of the Pd thin films is similar at ambient and UHV conditions. We have also shown that the microstructure of palladium films exposed to air at room temperature for STM imaging are not significantly affected by ambient gases, and they exhibit reproducible microstructure and catalyst activity. However, exposure of the film to reaction environment can have a significant impact on both microstructure and reactivity.

We have clearly demonstrated that catalytic surfaces can be strongly influenced by both pretreatment and reaction environments causing microstructural transformations that can significantly alter the activity of the surface resulting in subsequent changes in reaction kinetics. Activity and selectivity alteration coincided with the transition from one microstructure to another. These changes are attributed

to the varying active-site distribution caused by the transformation in surface structure.

Reaction results from three palladium films show that different microstructures in general exhibit different catalytic behavior, whereas similar microstructures usually have identical activity regardless of their treatment history, provided the composition remains the same.

ACKNOWLEDGMENTS

We gratefully acknowledge funds from NSF Grant CBT 88-06640 for the purchase of the STM and from NSF Grants CTS 90-015686 and CTS 92-15339 for supporting this reasearch.

REFERENCES

1. Yeung, K. L. and Wolf, E. E., *J. Catal.* **143,** 409 (1993).
2. Wang, T., Lee, C., and Schmidt L. D., *Surf. Sci.* **163,** 181 (1985).
3. Flytzani-Stephanopoulos, M., Wong, S., and Schmidt, L. D., *J. Catal.* **49,** 51 (1977)
4. Ruckenstein, E., and Sushumna, I., *in* "Hydrogen Effects in Catalysis: Fundamentals and Practical Applications (Z. Paal and P. G. Menon, Eds.). Dekker, New York, 1988.
5. Somorjai, G. A., "Chemistry in Two Dimensions Surfaces." Cornell Univ. Press, Ithaca, NY, 1981.
6. Kuk, Y., *in* "Scanning Tunneling Microscopy I" (H.-J. Guntherodt and R. Wiesendanger, Eds.). Springer-Verlag, New York, 1992.
7. Campbell, R. A., Guan, J., Madey, T. E., *Catal. Lett.*, in press.
8. Yeung, K. L., and Wolf, E. E., *Catal. Lett.* **12,** 213 (1992).
9. Yeung, K. L., and Wolf, E. E., submitted for publication.
10. Yeung, K. L., and Wolf, E. E., *J. Vac. Sci. Technol. B* **9,** 798 (1991).
11. Yeung, K. L., and Wolf, E. E., *J. Vac. Sci. Technol. A* **10,** 651 (1992).
12. Yeung, K. L., and Wolf, E. E., *J. Catal.* **135,** 13 (1992).
13. Cowans, B. A., Jurman, K. A., Delgass, W. N., Li, Y. Z., Reifenberger R. and Koch T. A., *J. Catal.* **125,** 501 (1990).
14. Humbert, A., Dayez, M., Granjeaud, S., and Ricci, P., *J. Vac. Sci Technol. B* **9**, 804 (1991).
15. Scholten, J. J. F., and Pijper, A. P., and Husting, A. M. L., *Catal. Rev. Sci. Eng.* **27,** 151 (1985).
16. Mullins, W. W., *in* Metal Surfaces: Structure Energetics and Kinetics" (W. D. Robertson, and N. A. Gjostein, Eds.) pp. 17–66. International, Materials, ASM, Materials Park, OH, 1962.
17. Dreschler, M., *in* Surface Mobilities on Solid Materials: Fundamental Concepts and Applications" (T. B. Vu, Ed.). Plenum, New York, 1983.
18. Shi, A.-C. and Masel, R. I., *J. Catal.* **120,** 421 (1989).
19. Lee, K.-H., and Wolf, E. E., *Catal. Lett.* **26,** 297 (1994).
20. McCabe, R. W., Pignet, T., and Schmidt, L. D., *J. Catal.* **32**, 114 (1974).
21. Rhead, G. E., and Mykura, H., *Acta Metall.* **10,** 843 (1962).
22. Geus, J. W., *in* "Material Science Research, Vol. 10" (G. C. Kuczynski, Ed.). Plenum Press, New York, 1975.
23. Avery, N. R., and Sheppard, N., *Surf. Sci. Lett.*, L367 (1986).
24. Pradier, C.-M., and Berthier, Y., *J. Catal.* **129,** 356 (1991).
25. Bertolini, J. C., and Massardier, J., *in* "The Chemical Physics of Solid Surfaces and Heterogeneous Catalysis, Vol. 3B" (D. A. King and D. P. Woodruff, Eds.), pp. 107–136. Elservier, New York, 1984.
26. Massadier, J., Bertolini, J. C., and Renouprez, A., *in* "Proceedings, 9th International Congress on Catalysis Calgary, 1988" (M. J. Phillips and M. Ternan, Eds.), Vol. 3, pp 1222–1229. Chem. Institute of Canada, Ottawa, 1988.
27. Tardy, B.,Noupa, C., Leclerq, C., Bertolini, J. C., Hoareau, A., Treilleux, M., Faure, J. P., and Nihoul, G., *J. Catal.* **129,** 1 (1991).
28. Strausser, Y. E., and Heaton, M. G., *Am. Lab.*, May 1994.